

NOTE TO USERS

**Duplicate page number(s); text follows.
The manuscript was scanned as received.**

40

This reproduction is the best copy available.

UMI[®]

PREVIEW

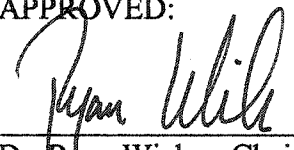
PREVIEW

**FLOW AND THERMAL ANALYSIS OF A COMPUTER CHASSIS
USING LIQUID CRYSTAL THERMOGRAPHY AND HOT-WIRE
ANEMOMETRY**

LUIS ALFONSO TERRAZAS

Department of Mechanical and Industrial Engineering

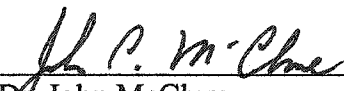
APPROVED:



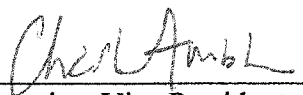
Dr. Ryan Wicker, Chair



Dr. Ahsan Choudhuri



Dr. John McClure



Associate Vice President
for Graduate Studies

PREVIEW

THIS THESIS IS DEDICATED TO MY PARENTS,

Luis and Carmen Terrazas:

In Whom I have found unending love and support.

PREVIEW

PREVIEW

**FLOW AND THERMAL ANALYSIS OF A COMPUTER CHASSIS
USING LIQUID CRYSTAL THERMOGRAPHY AND HOT-WIRE
ANEMOMETRY**

by

LUIS ALFONSO TERRAZAS, B.S.M.E.

THESIS

Presented to the Faculty of the Graduate School of
The University of Texas at El Paso
in Partial Fulfillment
of the Requirements
for the Degree of

MASTER OF SCIENCE

Department of Mechanical and Industrial Engineering

THE UNIVERSITY OF TEXAS AT EL PASO

August 2001

UMI Number: ep05548



UMI Microform ep05548

Copyright 2003 by ProQuest information and Learning Company.

All rights reserved. This microform edition is protected against
unauthorized copying under Title 17, United States Code.

ProQuest Information and Learning Company
300 North Zeeb Road
P.O. Box 1346
Ann Arbor, MI 48106-1346

Acknowledgments

I would like to thank Dr. Ryan Wicker, Director of the NASA Flow and Thermal Imaging Laboratory for giving me the opportunity to perform this research. Dr. Wicker deserves my sincere appreciation for the valuable support, and tremendous amount of time he dedicated to the development of this thesis. I would also like to thank Dr. Ahsan Choudhuri for all the feedback and guidance he provided during the writing of this thesis and Dr. John McClure for serving on my committee. Also, I would like to thank Dr. Christopher Elkins and Mr. Paul Kodzwa of Stanford University for providing some of the software used in this research. In addition, my sincere appreciation goes to Dr. Rolando Quintana, Chairman of the Mechanical and Industrial Engineering Department at UTEP for the support he provided to this research. Additionally, I would like to thank NASA and Dr. Po Wen-Hu at Axxion Group Corporation for the financial support provided for this project.

Several other people in the department deserve recognition. I would like to thank Rudy Aguilar, Carlos Herrera, Oscar Acosta, and Carrie McKillip for their assistance in the construction and purchase of numerous laboratory components. My co-workers in the laboratory, Hugo Loya, Fernando Jasso, Juvenal Herrera, David Candelas, have assisted me greatly in the completion of this work. Other student researchers that have contributed in one way or another throughout my graduate studies include Jorge Camacho, Frank Medina, Miguel Perez, Erasmo Lopez, and Robert Hennessey.

My family deserves my most sincere appreciation. Thank you Mom and Dad for the love and support you provided throughout my college career. My brother Jesus and my sister Marisela deserve my gratitude for keeping me motivated. Most especially I give thanks to my wife Esperanza for the tremendous amount of encouragement and support she provides for me everyday.

This thesis was submitted to the supervising committee on August 1, 2001.

PREVIEW

Executive Summary

This thesis describes the application of three well-established techniques for flow and temperature field characterization: liquid crystal thermography, smoke-wire flow visualization, and hot-wire anemometry. These techniques were used to investigate an alternative computer chassis configuration and compare its flow and temperature distribution to the original production chassis. The alternative configuration involved blocking all chassis orifices (including the vacant vent hole array on the backside of the chassis) with the exception of the original ventilation intake and exhaust. The modification of the chassis provided a means for demonstrating the effectiveness of using these experimental techniques in the electronic enclosure design process.

Full-field temperature measurements were obtained using liquid crystal thermography. This technique was developed as a relatively inexpensive tool used to visualize complex temperature distributions on solid surfaces. Liquid crystals react to changes in temperature by continuously changing color over an active range from 0.5 to 30 degrees Celsius in width. Liquid crystal imaging can easily provide qualitative full-field temperature information. Quantitative temperature information is obtainable by means of a calibration procedure that associates temperature with a measurable scalar that represents the color of the liquid crystal surface. Even though it is an intrusive technique, Hallcrest (1987) considers liquid crystal thermography to be the most suitable technique for measuring temperatures of electronic devices.

Flow field characterization of the chassis was performed using two techniques: smoke-wire flow visualization and hot-wire anemometry. First, a qualitative assessment of the flow structure was obtained using the smoke-wire. Second, the flow was quantified using a constant temperature hot-wire anemometer. The experimental techniques employed in and results obtained from this work are intended to be useful for the improvement of electronics cooling and chassis design practices.

The increasing power and performance of electronic components provide packaging engineers with an unending challenge to re-evaluate their current thermal design practices. The design of electronic enclosures faces a design dilemma between thermal management and electromagnetic interference (EMI) containment. Conventional electronic enclosure design practices are mostly responsive to consumer needs. High temperatures experienced by electronic components inside a computer are a concern for chassis designers. Research in this area using Computational Fluid Dynamics (CFD) software has become attainable with the advancement in computer technology. However, these computer models oftentimes do not account for parameters such as wire and ribbon cable size and location, and hence can yield inaccurate models.

Using the techniques mentioned above, several differences were found in the flow field structure of the original chassis configuration versus the alternative configuration. For example, flow near the vacant vent hole area was measured at ~ 1 m/sec in the original chassis configuration and ~ 0.5 m/sec in the alternative chassis. The flow velocity in the area close to the processor-cooling fan was also higher in the original

chassis configuration (~ 1 m/sec) than in the alternative configuration (~ 0.7 m/sec). These differences in the flow field structure within the chassis have a direct effect on the temperature of the components. For instance, the temperature of the ICH2 chip in the original chassis configuration was 38°C , which was 2°C higher than in the alternative chassis. The average temperature of the audio codec chip was 39.6°C in the original chassis configuration, an increase of 1.2°C compared to the same chip in the alternative configuration. The differences in the flow field structures of the two chassis configurations were further identified using a smoke-wire flow visualization technique. Images captured using this technique helped to determine the regions with higher velocity flow and provided a qualitative description of the direction of the flow. Using the smoke-wire, it was determined that the uncovered vent hole array in the original chassis configuration served as a “secondary” ventilation intake. That was not the case for the covered holes of the alternative configuration.

The results presented in this thesis show that these three well-established techniques can be applied to obtain valuable flow and temperature information to be used in the design process of electronic enclosures. Furthermore, the integration of these techniques into current design practices can provide experimental validation for numerical models of the flow and temperature fields within the chassis.

Table of Contents

Acknowledgments.....	iv
Executive Summary	vi
Table of Contents	ix
List of Tables	xiii
List of Figures	xiv
Chapter 1 Introduction	1
1.1 Project Overview	1
1.2 Project Objectives	2
1.3 Research Motivation	3
1.4 Laboratory Involved.....	4
1.5 Thesis Outline	6
Chapter 2 Literature Survey.....	7
2.1 Introduction.....	7
2.2 Thermal Imaging.....	7
2.2.1 Infrared Thermography.....	8
2.2.2 Liquid Crystal Thermography.....	9
2.3 Liquid Crystals.....	9
2.3.1 Introduction.....	9
2.3.2 Nematic, Chiral Nematic, and Smectic Liquid Crystals	12

2.3.3	Optical Properties of Liquid Crystals	14
2.3.3.1	Textures.....	14
2.3.3.2	Polarization	16
2.3.3.3	Reflection and Refraction	17
2.3.3.4	Birefringence.....	17
2.3.4	Temperature Sensitivity of Liquid Crystals.....	18
2.3.5	Quantitative Color Representation.....	20
2.3.6	Calibration of Thermochromic Liquid Crystals.....	22
2.3.7	LC Thermography and Other Applications of Liquid Crystals	25
2.4	Design of Computer Chassis and Thermal Management	27
2.5	Smoke-Wire Flow Visualization.....	31
2.6	Hot-Wire Anemometry	33
2.6.1	Hot-Wire Configuration.....	34
2.6.2	Hot-Films	37
2.6.3	Calibration of Hot-Wires and Hot-Films	38
2.7	Computational Fluid Dynamics	39
Chapter 3 Experimental Setup and Procedures.....		40
3.1	Introduction.....	40
3.2	Experimental Setup.....	40
3.2.1	Test Chassis	40
3.2.2	Board preparation and TLC application	43

3.2.3	Imaging System	48
3.2.4	Hot-Wire Anemometry System	53
3.2.5	Liquid Crystal Calibration System.....	54
3.2.6	Hot-Wire Calibration System	56
3.3	Laboratory Software and Procedures.....	58
3.3.1	Laboratory Software	58
3.3.1.1	LabVIEW.....	59
3.3.1.2	Thermal Pro Software for IFA 300 Anemometer.....	62
3.3.1.3	Tecplot	63
3.3.2	Experimental Procedures	63
3.3.2.1	Liquid Crystal Calibration Procedure	63
3.3.2.2	Hot-Wire Calibration Procedure.....	65
3.3.2.3	Temperature Measurement Procedure	69
3.3.2.4	Smoke-Wire Flow Visualization.....	70
3.3.2.5	Hot-Wire Velocity Measurement Procedure	72
3.4	Uncertainty Analysis.....	73
Chapter 4 Effect of Vacant Chassis Inlets on Flow Field Structure and Motherboard		
Temperature		75
4.1	Chapter Summary	75
4.2	Full-field Motherboard Temperature	76
4.2.1	Original Chassis Configuration.....	77

4.2.2	Alternative Chassis Configuration	88
4.2.3	Motherboard Temperature Comparisons	98
4.3	Smoke-Wire Flow Visualization.....	101
4.4	Flow Field Characterization.....	104
4.4.1	Flow Velocity and Turbulence Intensity Profiles	106
Chapter 5 Conclusions and Recommendations.....		126
5.1	Conclusions.....	126
5.2	Recommendations.....	129
References.....		129
Appendix A.....		140
Appendix B		141
Appendix C		142
Appendix D.....		178
Curriculum Vitae		182

List of Tables

Table 3.1.	Equipment used in experimental setup.	51
Table 3.2.	Summary of experimental programs.....	60
Table 3.3.	Calibration Methods for IFA 300 Anemometer.....	67
Table 3.4.	Nominal operating conditions inside laboratory.....	69

PREVIEW

List of Figures

Figure 2.1.	Schematic illustration of the solid, liquid crystal, and liquid phases. The slender lines represent molecules; adapted from Collings (1990).	12
Figure 2.2.	Nematic liquid crystal sample between crossed polarizers.....	13
Figure 2.3.	Chiral Nematic liquid crystal sample between crossed polarizers.....	14
Figure 2.4.	The Chiral Nematic liquid crystal structure.....	15
Figure 2.5.	Orientation of helical and molecular axes relative to incident light.	18
Figure 2.6.	Electrical Circuit Diagram of: a) Constant Current Anemometer b) Constant Temperature Anemometer	35
Figure 2.7.	Common hot-wire probe configurations a) Normal single wire. b) Crossed wire. c) Triple wire.	36
Figure 3.1.	Overall schematic of the hot-wire anemometry and liquid crystal thermography systems.	41
Figure 3.2.	Gateway Performance series computer chassis.	42
Figure 3.3.	a) Non-Conductive black ink and thermochromic liquid crystals b) Aztek A470 airbrush.....	44
Figure 3.4.	Wilkerson air purge components for regulating and controlling air.....	45
Figure 3.5.	Intel D815EE1 ATX motherboard used for experiments, a) In its original configuration. b) After being coated with black ink and liquid crystals...	46
Figure 3.6.	Intel D815EE1 motherboard component location.	47

Figure 3.7.	a) Edmund Scientific R30C5W liquid crystal sheet. b) Heitronics Reference IR pyrometer.	48
Figure 3.8.	Arrangement of imaging system.	50
Figure 3.9.	Hot-wire anemometry system.	54
Figure 3.10.	TLC in-situ calibration system.	56
Figure 3.11.	Wind tunnel used for hot-wire calibration.	57
Figure 3.12.	a) Setra 264 pressure transducer. b) Dwyer 1430 micro-manometer.	66
Figure 4.1.	Black ink and TLC coated motherboard with highlighted ROI 1.	82
Figure 4.2.	Temperature map of ROI 1 in the original chassis configuration.	82
Figure 4.3.	Black ink and TLC coated motherboard with highlighted ROI 2.	83
Figure 4.4.	Temperature map of ROI 2 in the original chassis configuration.	83
Figure 4.5.	Black ink and TLC coated motherboard with highlighted ROI 3.	84
Figure 4.6.	Temperature map of ROI 3 in the original chassis configuration.	84
Figure 4.7.	Black ink and TLC coated motherboard with highlighted ROI 4.	85
Figure 4.8.	Temperature map of ROI 4 in the original chassis configuration.	85
Figure 4.9.	Black ink and TLC coated motherboard with highlighted ROI 5.	86
Figure 4.10.	Temperature map of ROI 5 in the original chassis configuration.	86
Figure 4.11.	Black ink and TLC coated motherboard with highlighted ROI 6.	87
Figure 4.12.	Temperature map of ROI 6 in the original chassis configuration.	87
Figure 4.13.	Black ink and TLC coated motherboard with highlighted ROI 1.	92
Figure 4.14.	Temperature map of ROI 1 in the alternative chassis configuration.	92

Figure 4.15.	Black ink and TLC coated motherboard with highlighted ROI 2.....	93
Figure 4.16.	Temperature map of ROI 2 in the alternative chassis configuration.	93
Figure 4.17.	Black ink and TLC coated motherboard with highlighted ROI 3.....	94
Figure 4.18.	Temperature map of ROI 3 in the alternative chassis configuration.	94
Figure 4.19.	Black ink and TLC coated motherboard with highlighted ROI 4.....	95
Figure 4.20.	Temperature map of ROI 4 in the alternative chassis configuration.	95
Figure 4.21.	Black ink and TLC coated motherboard with highlighted ROI 5.....	96
Figure 4.22.	Temperature map of ROI 5 in the alternative chassis configuration.	96
Figure 4.23.	Black ink and TLC coated motherboard with highlighted ROI 6.....	97
Figure 4.24.	Temperature map of ROI 6 in the alternative chassis configuration.	97
Figure 4.25.	Chassis areas investigated using smoke-wire flow visualization.	102
Figure 4.26.	Flow structure in vent hole array area for: a) Original configuration b) Alternative configuration	103
Figure 4.27.	Flow structure in power supply fan area for: a) Original configuration b) Alternative configuration	103
Figure 4.28.	Flow structure in expansion slot area for: a) Original configuration b) Alternative configuration	104
Figure 4.29.	a) Side view of modified chassis used to profile velocity. b) Front view of modified chassis used to profile velocity, c) Isometric view of modified chassis used to profile velocity.	106

- Figure 4.30.** a) Covered Chassis slot 1 x-y plane 0-degree flow. b) Covered Chassis slot 1 x-y plane 90-degree flow. c) Uncovered Chassis slot 1 x-y plane 0-degree flow. d) Uncovered Chassis slot 1 x-y plane 90-degree flow. 112
- Figure 4.31.** a) Covered Chassis slot 1 x-y plane 0-degree flow. b) Covered Chassis slot 1 x-y plane 90-degree flow. c) Uncovered Chassis slot 1 x-y plane 0-degree flow. d) Uncovered Chassis slot 1 x-y plane 90-degree flow. 113
- Figure 4.32.** a) Velocity distribution for slot 1, $y=0.245$ m. in x-y plane. b) Turbulence intensity for slot 1, $y=0.245$ m. in x-y plane. 114
- Figure 4.33.** a) Covered Chassis slot 1 x-y plane 0-degree turbulence intensity. b) Covered Chassis slot 1 x-y plane 90-degree turbulence intensity. c) Uncovered Chassis slot 1 x-y plane 0-degree turbulence intensity. d) Uncovered Chassis slot 1 x-y plane 90-degree turbulence intensity. 115
- Figure 4.34.** a) Covered Chassis slot 4 x-y plane 0-degree flow. b) Covered Chassis slot 4 x-y plane 90-degree flow. c) Uncovered Chassis slot 4 x-y plane 0-degree flow. d) Uncovered Chassis slot 4 x-y plane 90-degree flow. 116
- Figure 4.35.** a) Covered Chassis slot 4 x-y plane 0-degree flow. b) Covered Chassis slot 4 x-y plane 90-degree flow. c) Uncovered Chassis slot 4 x-y plane 0-degree flow. d) Uncovered Chassis slot 4 x-y plane 90-degree flow. 117
- Figure 4.36.** a) Covered Chassis slot 4 x-y plane 0-degree turbulence intensity. b) Covered Chassis slot 4 x-y plane 90-degree turbulence intensity. c)

	Uncovered Chassis slot 4 x-y plane 0-degree turbulence intensity. d)	
	Uncovered Chassis slot 4 x-y plane 90-degree turbulence intensity.	118
Figure 4.37.	a) Covered Chassis slot 6 x-y plane 0-degree flow. b) Covered Chassis slot 6 x-y plane 90-degree flow. c) Uncovered Chassis slot 6 x-y plane 0-degree flow. d) Uncovered Chassis slot 6 x-y plane 90-degree flow.	119
Figure 4.38.	a) Covered Chassis slot 6 x-y plane 0-degree flow. b) Covered Chassis slot 6 x-y plane 90-degree flow. c) Uncovered Chassis slot 6 x-y plane 0-degree flow. d) Uncovered Chassis slot 6 x-y plane 90-degree flow.	120
Figure 4.39.	a) Velocity distribution for slot 6, $y=0.254$ m. in x-y plane. b) Turbulence intensity for slot 6, $y=0.254$ m. in x-y plane.....	121
Figure 4.40.	a) Covered Chassis slot 6 x-y plane 0-degree turbulence intensity. b) Covered Chassis slot 6 x-y plane 90-degree turbulence intensity. c) Uncovered Chassis slot 6 x-y plane 0-degree turbulence intensity. d) Uncovered Chassis slot 6 x-y plane 90-degree turbulence intensity.	122
Figure 4.41.	a) Covered Chassis slot 8 x-y plane 0-degree flow. b) Covered Chassis slot 8 x-y plane 90-degree flow. c) Uncovered Chassis slot 8 x-y plane 0-degree flow. d) Uncovered Chassis slot 8 x-y plane 90-degree flow.	123
Figure 4.42.	a) Covered Chassis slot 8 x-y plane 0-degree flow. b) Covered Chassis slot 8 x-y plane 90-degree flow. c) Uncovered Chassis slot 8 x-y plane 0-degree flow. d) Uncovered Chassis slot 8 x-y plane 90-degree flow.	124

Figure 4.43.	a) Covered Chassis slot 8 x-y plane 0-degree turbulence intensity. b) Covered Chassis slot 8 x-y plane 90-degree turbulence intensity. c) Uncovered Chassis slot 8 x-y plane 0-degree turbulence intensity. d) Uncovered Chassis slot 8 x-y plane 90-degree turbulence intensity.	125
Figure A.1.	Calibration plot for R30C10W thermochromic liquid crystals.....	140
Figure A.2.	Calibration plot for R40C5W thermochromic liquid crystals.....	140
Figure B.1.	Pressure transducer calibration.	141
Figure B.2.	Hot-Film Calibration.....	141
Figure C.1.	a) Velocity distribution for slot 1, $y=0.305$ m. in x-y plane. b) Turbulence intensity for slot 1, $y=0.305$ m. in x-y plane.....	142
Figure C.2.	a) Velocity distribution for slot 1, $y=0.279$ m. in x-y plane. b) Turbulence intensity for slot 1, $y=0.279$ m. in x-y plane.....	143
Figure C.3.	a) Velocity distribution for slot 1, $y=0.254$ m. in x-y plane. b) Turbulence intensity for slot 1, $y=0.254$ m. in x-y plane.....	144
Figure C.4.	a) Velocity distribution for slot 1, $y=0.228$ m. in x-y plane. b) Turbulence intensity for slot 1, $y=0.228$ m. in x-y plane.....	145
Figure C.5.	a) Velocity distribution for slot 1, $y=0.203$ m. in x-y plane. b) Turbulence intensity for slot 1, $y=0.203$ m. in x-y plane.....	146
Figure C.6.	a) Velocity distribution for slot 1, $y=0.177$ m. in x-y plane. b) Turbulence intensity for slot 1, $y=0.177$ m. in x-y plane.....	147